Analysis of potential improvements in the performance of solenoid injectors in diesel engines

Indexed by:
Web of Science Group

Oleksandr Vrublevskyi[a], Sławomir Wierzbicki[a,*]

[a] University of Warmia and Mazury in Olsztyn, Faculty of Technical Sciences, Olsztyn, Poland,

Highlights

- high-speed solenoid injector;
- mathematical model of a solenoid valve;
- new technology for manufacturing magnetic cores;

Abstract

Efficient fuel injection and exhaust gas cleaning systems are needed to promote the development of high-performance internal combustion systems and decrease greenhouse gas emissions. Electronically controlled injection systems enable nearly unlimited control over system components whose operation is limited by the inertia of moving parts and other physical phenomena. In the present study, a novel technology for manufacturing magnetic cores was proposed to improve the performance of solenoid injectors in Diesel engines. The conducted simulations and experiments revealed that the developed technology can increase the speed of solenoid injectors. In the proposed solution, the fuel dose was split to effectively control the injection process and improve engine performance.

Keywords
diesel engine, solenoid injector, solenoid valve, electromagnetic circuit

1. Introduction

The Fit for 55 package has been introduced by the European Union to reduce greenhouse emissions by 55% by 2030 (relative to 1990 levels) and make the EU climate neutral by 2050 [20]. Emissions should also be controlled in the transport industry which is one of the largest contributors to greenhouse gas emissions. The above applies particularly to Diesel engines which emit more nitric oxide (NOx) compounds and particulate matter (PM) than internal combustion engines [2]. However, Diesel engines are much more efficient, and they are widely used in vans, delivery trucks, and heavy-duty machines. Most research on the performance of Diesel engines has been conducted to improve the efficiency of exhaust gas cleaning systems [24, 30, 36], to increase the share of biodiesel in the diesel blend [10, 12] and improvement of road safety [5, 6].

Greenhouse gas emissions from Diesel engines can also be reduced by improving the precision of fuel metering and controlling the combustion process in cylinders. In Diesel engines, combustion is strictly determined by fuel injection characteristics. Modern Diesel engines are equipped with high-pressure Common Rail (CR) systems that optimize fuel delivery and split the fuel dose into several injection pulses. Split injection enables effective combustion control and reduces toxic emissions [15, 35]. According to Stelmasiak et al. [25], the volume and timing of the pilot injection and post injections influence engine performance parameters.

The structure of a fuel injection has to be optimized to increase engine performance and reduce greenhouse gas emissions. Fuel injection parameters determine spray

(*) Corresponding author.
E-mail addresses: O. Vrublevskyi (ORCID: 0000-0002-5871-6381) aleksander.wroblewski@uwm.edu.pl,
                      S. Wierzbicki (ORCID: 0000-0002-5935-6613) slawekw@uwm.edu.pl

penetration in the cylinder and fuel metering during operation. Mathematical equations describing the physical phenomena inside a fuel injector have been presented, and novel solutions have been proposed in the literature.

Fuel metering, in particular injection timing, poses a key problem in research studies aiming to improve the combustion efficiency of Diesel engines. Highly dynamic mechanical, hydraulic, and electrical processes inside an injector have to be precisely described to accurately determine the beginning and end of fuel injection [8, 11]. According to many researchers, the duration of injection is equivalent to the electric pulse controlling a solenoid valve inside the injector [4, 19]. However, this is a highly simplified assumption, and complex phenomena that accompany fuel injection should be taken into consideration in in-depth analyses. It should also be noted that the electric signal that leads to the displacement of the injector needle is difficult to measure not only in Diesel engines, but also in internal combustion engines [29] and gaseous fuel injectors [34].

The complex phenomena inside a fuel injector have to be analyzed in detail, and the displacement of an injector's moving parts has to be accurately measured to determine the temporal relationships between the electric pulse applied to the coil and the fuel injection process. The displacement of an injector's moving parts is difficult to measure not only because these elements are difficult to access, but also because displacement values are very small. The maximum displacement of the plunger inside the magnetic coil is around 50 μm, and needle displacement is 100-600 μm [23, 32], which is why dedicated measuring systems are required.

Hydraulic and mechanical processes inside injectors have been relatively well described and researched, which is why the range of potential improvements in an injector's mechanical components is limited. However, the impact of electromagnetic phenomena on an injector's performance has been disregarded in most fuel injector models proposed in the literature. For example, Hu et al. [13] developed a model of a fuel injector in Amesim software, but they focused solely on the impact of fuel parameters on injector performance and found that fuel density and viscosity influenced the injection rate. They analyzed hydraulic processes in the injector, but disregarded electromagnetic phenomena in the coil, which also play an

important role in injector performance. In turn, Martínez-Martínez et al. [18] analyzed the amount of injected fuel at different dwell times between injection pulses. They concluded that dwell times between successive electric pulses significantly influence the amount of delivered fuel. The performance of a solenoid valve in a fuel injector was examined by Huber and Ulbrich [14] who developed a test bench to measure magnetic field strength at different air gap values and proposed an empirical model of a solenoid valve. They concluded that the impact of eddy currents, which are generated when the supply current is switched on and off, cannot be disregarded. Ando et al. [1] also observed that magnetic phenomena in the coil influence the dynamic characteristics of a fuel injector. Based on the developed model, they concluded that eddy currents, magnetic saturation, magnetic properties of the core, and magnetic hysteresis should be taken into consideration to increase fuel metering precision. Zhao et al. [38] analyzed electromagnetic phenomena in a fuel injector, but their study was limited to measuring magnetic field distribution, power losses, and the impact of the electric pulse on injector opening time. They developed a model of a fuel injector with the use of the finite element method (FEM), but they did not examine the impact of different magnetic materials on injector performance [31]. In turn, Piron et al. [22] proposed a mathematical model of a fuel injector to describe two magnetization characteristics at extreme positions of a solenoid valve and develop interpolation functions for intermediate positions of the valve. The model supported fast computation, but the presented solution was a compromise between accuracy and computation speed.

A review of the literature on electromagnets developed for various applications indicates that their performance can be improved by modifying injection control, applying novel materials and production technologies. In the work of Zhao et al. [39], electromagnets made of soft magnetic materials improved the modeled and real-world performance of a fuel injector. In a different study, Zhao et al. [40] performed a finite element simulation of a fuel injector and observed that the control pulse should be adapted to the properties of magnetic materials to optimize valve control.

A review of the literature suggests that the physical properties of the materials applied in a solenoid valve, in

particular the magnetic core, pose the greatest obstacle to improving the performance of solenoid injectors. Therefore, new technologies for manufacturing magnetic cores in solenoid valves should be developed to improve valve response times and control fuel injection with greater precision.

2. Description of the analyzed object and measurement technique

2.1 Solenoid injector

Most Common Rail systems are equipped with solenoid injectors. The structure of a solenoid injector is presented in Figure 1 [26-27].
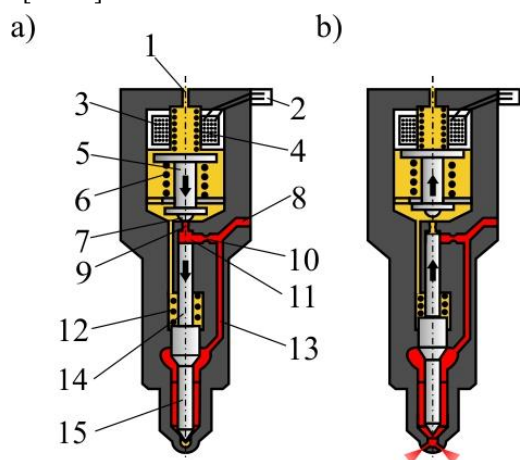

Figure 1. Cross-section of a Bosch solenoid injector in 1st and 2nd generation Common Rail systems: a) injector closed, b) fuel injection into the combustion chamber: 1 – drain orifice, 2 – electrical connector, 3 – coil, 4 – upper plunger spring, 5 – piston, 6 – lower plunger spring, 7 – ball value, 8 – high pressure fuel supply channel, 9 – drain gland, 10 -inlet gland, 11 – control chamber, 12 – spray nozzle spring, 13 – fuel supply line, 14 – control piston, 15 – nozzle needle [32].

When the injector is closed (Fig. 1a), voltage is not applied to the coil (3), and high fuel pressure in the control chamber (11) (which acts on the control piston (14)) and the force of the nozzle spring (12) act on the needle (15). The sum of these forces significantly exceeds the force exerted by high fuel pressure on the conical end of the needle. When voltage is applied to the coil, the control valve piston (5) is displaced by the generated electromagnetic field, and fuel flows from the control chamber to the drain orifice (1). The drain orifice (1) has a larger diameter than the drain gland (9), and the resulting difference in pressure causes the needle to move up and opens the nozzle.

2.2. Control pulse characteristics

The power supply circuit of a solenoid valve coil which generates the electric pulse is presented in Figure 2.
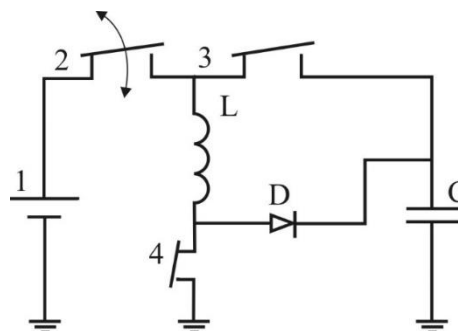

Figure 2. Diagram of the power supply circuit of a solenoid injector: 1 – battery; 2 – spring tensioner; 3, 4 – switches; L – injector coil; D – diode; C – capacitor.

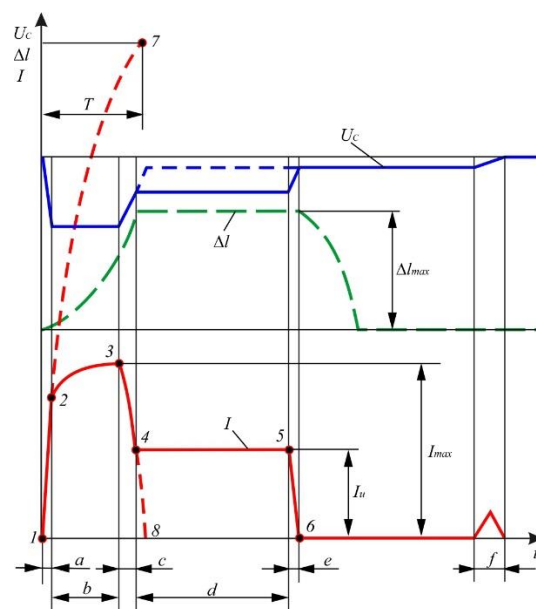The control pulse generated by the power supply circuit is presented in Figure 3.

Figure 3. Control pulse supplied to the injector coil: U_c – capacitor voltage; I_a – current passing through the coil; Δl – armature displacement.

The control pulse is divided into six phases: a – initial phase; b – opening phase; c – transitional phase; d – maintenance phase; e – closing phase; f – capacitor charging phase.

In phase a, the capacitor C supplies voltage U_c to the injector coil L (Fig. 2). The magnetic circuit is fully saturated in time T (time constant), and the current I applied to the coil L can reach 200 A or more at time T (curve 1-7). Time T is around 0.1-0.2 ms, and in the analyzed case, the current applied to the coil is much smaller because the coil switches to battery supply in point 2. The piston is set in motion Δl in phase b. If injection

has to be stopped in this phase (0.1-0.5 ms), the condenser C in connected in point 3, and current I decreases rapidly (phase 3-4-8). Injection times longer than 0.35 ms have a maintenance phase d. In this case, current I decreases until point 4 and remains stable at $I_u \approx 0.5\ I_{max}$ between points 4 and 5. In point 5, voltage is no longer supplied, and the current in the coil decreases to zero (phase e). The capacitor is charged by the battery in transitional phases c and e, and it is also charged in phase f (Fig. 3) between fuel injections.

If injection time does not exceed 0.35 ms, the current in the coil has to be reduced to 300 A. In the analyzed power supply circuit, maximum current I in the coil was determined by the time interval between successive pulses τ (Fig. 4). Current I decreased by 3 A during the transition from idle operation ($\tau = 120$ ms) to near-nominal operation ($\tau = 40$ ms).
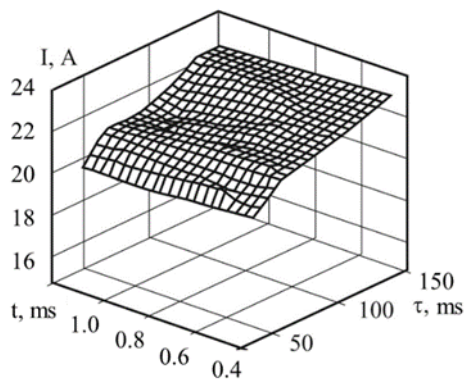

Figure 4. Changes in the maximum current in a solenoid valve coil depending on the duration of the control pulse and dwell time between pulses.

In addition to the power supply circuit, the materials used in the magnetic circuit also affect solenoid performance. The applied materials should maximize the magnetomotive force F_{mag}, while minimizing the impact of eddy currents and magnetic hysteresis.

Eddy currents lead to the uneven distribution of the magnetic flux in the cross-section of a magnetic circuit. The magnetizing force of eddy currents flowing in the direction of the main flux is greatest in the central part of the magnetic circuit where the number of eddy current loops is highest. At high frequencies, the magnetic flux penetrates only the thin surface layer of the control piston, which decreases apparent magnetic permeability (average in the cross-section). The tendency of a high-frequency magnetic flux to move away from ferromagnetic materials is known as the skin effect. The skin

effect increases the time constant T. According to the Joule-Lenz law, the heat released when an eddy current passes through a conductor leads to energy loss in a magnetic circuit.

The materials applied in the solenoid valves of fuel injectors are exposed to rapidly changing magnetic fields, which leads to magnetic circuit heating. The realignment of magnetic domains in these materials leads to internal friction, which produces heat. In each cycle, energy is dissipated as heat, and energy loss is proportional to the area of the hysteresis loop. Materials with low magnetic coercivity should be applied to reduce the area of the hysteresis loop. Hysteresis behavior is not observed in superparamagnetic materials (Fig. 5) with single-domain grains. These materials are composed of particles with a size of 10-15 nm.

Figure 5. View of the experimental magnetic cores.

Magnetic cores for the experiment were produced by sintering soft and hard magnetic materials. The grains of hard magnetic materials were coated with a dielectric adhesive and placed in soft magnetic material. Magnetic cores were sintered in a magnetic field to align magnetic domains in the core. The grains of hard magnetic materials were incorporated into soft magnetic material to increase the rate of magnetic field propagation and, consequently, to increase the speed of moving elements in the solenoid valve. Samples with various proportions of hard magnetic materials were used in the experiment.

The novel technology of producing a magnetic circuit with the use of soft (SM) and hard (HM) magnetic materials in a dielectric adhesive delivered the expected result by increasing the response rate of the solenoid valve. Winding speed was correlated with the proportion of hard magnetic material in the magneto-dielectric and the initial orientation of SM and HM domains. Five different magnetic cores were analyzed in the experiment. The first core was made of Armco iron which is

used in the production of solenoids for various applications. The second core was composed of high-purity (98%) iron insulated with a dielectric (dielectric content – 2-3%). In the remaining three cores, the content of HM grains in the SM material was 5%, 10%, and 15%. The content of the insulating dielectric adhesive was 2-3% in all three cores.

The magnetization curves of magneto-dielectrics for the injector's magnetic circuit are presented in Figure 6.
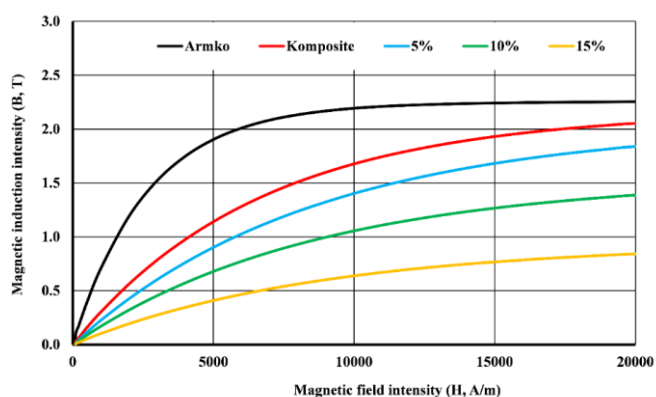

Figure 6. *B-H* magnetization curves.

Magnetic flux density B of $1.4 \div 1.9$ T in the region of magnetic induction was achieved when magnetic field strength was $H = 40 \div 100$ kA/m. The magnetic field generated by an electromagnet fluctuates, and the *B-H* magnetization curve forms a hysteresis loop. Magnetic hysteresis significantly influences injector dynamics. Due to magnetic field fluctuations, the magnetic circuit is not fully saturated, and a non-saturated hysteresis loop is difficult to model.

Measurement of piston displacement

The solenoid valve piston inside the control chamber is flushed with fuel from clearances and the control chamber during injector operation. The upper part of the piston enters the magnetic circuit of the coil with a maximum displacement of 50 μm. A tensiometer sensor with two perpendicular bars (Fig. 7) was designed to measure piston displacement with high precision and to minimize the impact of other processes during piston movement during the measurement [19]. The measuring bar (2) in the tensiometer was made of fiberglass with a high attenuation coefficient to minimize vibration. The bar was attached to the housing with screws, and the sensor shaft (3) was connected to the center of intersecting bars (2) at the top and to the piston at the bottom (6). A tensiometer (1) was glued on the surface of the bar to measure the strain caused by the moving

piston. Bar strain caused by the moving piston was measured with the use of a tensiometer glued onto the bar. Fiberglass thickness was selected to measure linear displacement within the examined range of values (0-50 μm). Fiberglass is paramagnetic, and this material was selected because the measuring bar was located near the coil generating a magnetic field with a flux density of up to 2.5 T. To increase measurement sensitivity, the system was bridged by two active tensiometric sensors. A layer of varnish was applied to the tensiometers to prevent direct contact with fuel.

The sensor shaft (3) was made of titanium to increase measurement accuracy and resistance to an extreme operating environment. Titanium is a paramagnetic material, and the shaft was made of titanium characterized by low density (4.51 g/cm^3), high elastic modulus ($110,000$ N/mm^2), and high linear thermal expansion coefficient (8.3×10^{-6} mm/K).

The signal received from the bridge diagonal was fed to the amplifier and filtered by removing the carrier component and amplifying the useful component. The amplified signal was transmitted by a L-783 ADC converter and registered by a computer. Detailed information about the sensor's design and the validation test was presented in the authors' previous study [32].
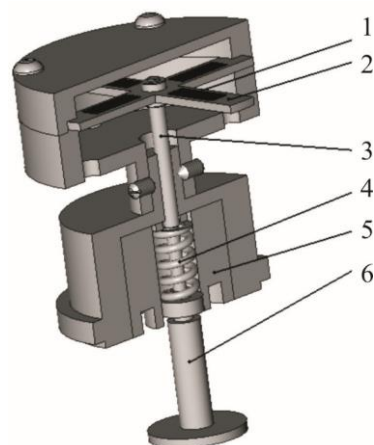

Figure 7. Piston displacement sensor: 1 – tensiometer, 2 – bar, 3 – shaft, 4 – valve spring, 5 – magnetic circuit, 6 – piston.

The measurements were conducted to compare the behavior of different core materials in the magnetic circuit. A control pulse composed of a short pulse (0.3 ms) and the main pulse (0.8 ms) was applied to initiate a two-stage fuel injection process. As a result, the performance of the solenoid valve under different conditions, including maximum winding speed and optimal force, could be analyzed during a single measurement.

The experiment was performed with different values of initial spring tension F_{sp} in the electromagnet and different magnetic materials.

Winding speed characteristics of the short control pulse and three selected samples are presented in Figure 8.
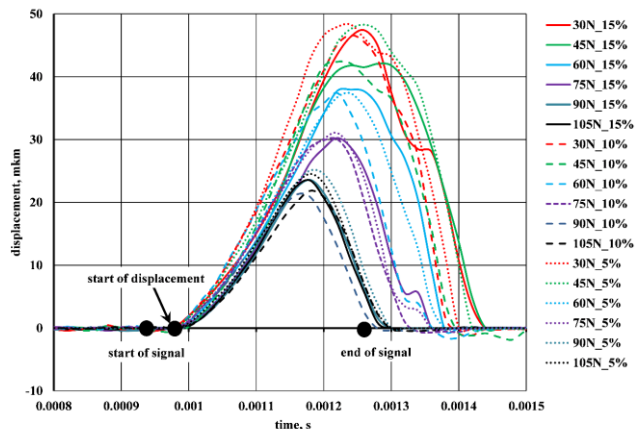

Figure 8. Displacement of the solenoid armature.

The analysis revealed that Fsp and core material significantly influenced armature displacement. At the initial length of the air gap (0.12 mm), maximum armature displacement was observed at the smallest Fsp of 30 N. The rate of armature displacement $Carh$ (Fig. 9) determines the time required to achieve a minimal distance between the armature and the magnetic circuit, which confirms the hypothesis that $Carh$ can be increased by adding hard magnetic material to the core.

The curves illustrating changes in average winding speed at different values of initial spring strain for a 0.2 ms pulse and maximum coil current of 25 A are presented in Figure 9.
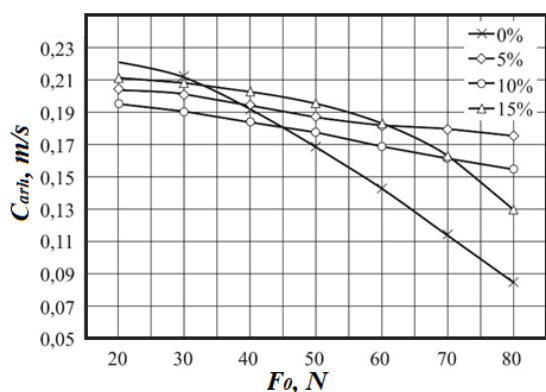

Figure 9. Average armature speed for magnetic cores with different proportions of hard magnetic materials.

The novel technology of producing a magnetic circuit with the use of SM and HM materials in a dielectric adhesive delivered the expected result by increasing the winding speed. Winding speed was also influenced by the proportion of HM grains in the magneto-dielectric and the initial orientation of magnetic domains in SM and HM materials. The characteristic value of initial spring strain F_0 was 40 N. At this value, winding speed was identical for magnetic circuits with and without the addition of HM material. At lower values of F_0, the addition of MT material decreased average winding speed. Winding speed in, a magnetic circuit with the addition of MT material increased with a rise in F_0 (at $F_0 = 70$ N, winding speed increased from 0.115 to 0.16 m/s). Therefore, the experiment confirmed that the proposed method of manufacturing magnetic cores is suitable for high-speed electromagnets.

3. Model of a solenoid value

A review of the literature [8, 18, 32, 33] indicates that hydrodynamic parameters are monitored in numerical models and experimental analyses of electronically controlled injectors. However, the specificity of electrodynamic processes in an injector's moving parts has not been considered in the existing research. Therefore, an accurate mathematical model should be developed to optimize an electromagnet's operating parameters, including the magnetic circuit, winding, and maximum and minimum air gap length. The optimal technologies for manufacturing solenoid valve components should also be specified.

Passarini et al. [21] analyzed the influence of fuel flow in a solenoid valve on armature displacement, initial spring tension, and friction forces. Koch et al. [17] analyzed a short-pulse nonlinear magnetic field at different voltages applied to the electromagnetic coil with the use of the FEM. This approach supported fast and accurate determination of magnetic field lines generated by the electromagnet. However, certain effects, mainly nonlinear effects, are not taken into consideration in the FEM. These effects include the magnetic saturation of the core, hysteresis, eddy currents in the magnetic circuit, and the magnetic permeability of the air gap. Two models can be applied simultaneously to analyze these effects: a dynamic model based on magnetic circuit equations and a solenoid model developed with the use of the FEM [28, 40]. Armature displacement induces changes in the geometry of a magnetic circuit, and every change has to be taken into account in the

FEM model. In the analyzed case, the armature was displaced at an estimated time of 0.1 ms, and the FEM model had to be adjusted to the solenoid's geometry to calculate the magnetic force. When *Fmag* is known, the solenoid's geometry is recalculated in the dynamic model, and the calculations are repeated. The implemented procedure is quite laborious and requires considerable computing power.

Passarini et al. [21] relied on Maxwell's equations describing electromagnetic processes to calculate magnetic field strength. Magnetic saturation, eddy currents, and hysteresis are taken into consideration in this approach.

An analysis of the diagrams of fuel injectors with a solenoid valve revealed that a mathematical model of a solenoid with armature displacement of 20-60 μm at a frequency of 50-60 Hz is required to develop equations for calculating electrohydrodynamic fuel flow. Solenoid valves that meet the above requirements are classified as fast response solenoids. A diagram of the magnetic circuit of a direct current electromagnet is presented in Figure 10.
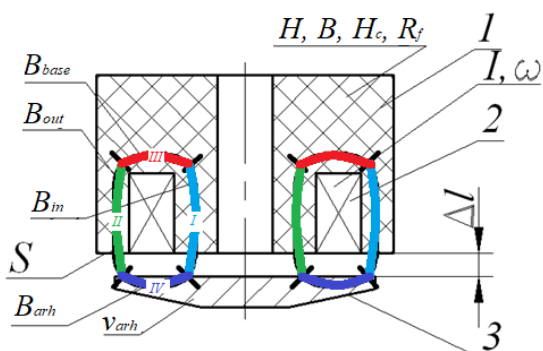

Figure 10. Diagram of a solenoid valve: 1 – magnetic circuit; 2 – coil; 3 – armature.

The parameters of the air gap have to be determined to calculate a solenoid's magnetic circuit and dynamics. Magnetic flux lines were determined based on several phenomena. Due to the presence of internal transverse forces in a magnetic field, magnetic flux lines tend to occupy the largest possible area and form convex curves around the poles. In the analyzed solenoid, convex curves were observed around the air gap and, partly, the orifice.

The heat transfer coefficient σ was calculated with the use of equation (1) to account for the presence of a leakage flux in the magnetic circuit:

$$\Phi(x) = \Phi_{arm} \cdot \left[1 + \frac{g_s}{G_{\text{н}}} \cdot \frac{x}{2} \cdot \left(2 - \frac{x}{l_s}\right)\right], \qquad (1)$$

where: $\Phi(x)$ – total flux in the magnetic circuit; Φ_{arm} – armature flux; g_s – magnetic permeability of the core; $G_{\text{н}}$ – total magnetic permeability of air gaps; l_s – coil length.

Equation (1) was integrated to obtain a formula for calculating σ:

$$\sigma = 1 + \frac{1}{3} \cdot \frac{g_s}{G_{\text{н}}}. \qquad (2)$$

Eddy currents and the hysteresis of the magnetic core were taken into consideration in the proposed model.

Equilibrium in the electric circuit was calculated with the use of equation (3).

$$U \cdot I = R \cdot I^2 - S \cdot \frac{B^2}{\mu_0} \cdot \frac{d\Delta l}{dt} + S \cdot l_k \cdot H_c \cdot \frac{dB}{dt} + \frac{dP}{dt} + R_f \cdot I_{ind}^2 \qquad (3)$$

where: $R \cdot I^2$ - loss of power caused by circuit resistance; $R_f \cdot I_{ind}^2$ - loss of power caused by induced current in the armature; $S \cdot \frac{B^2}{\mu_0} \cdot \frac{d\Delta l}{dt}$ – armature acceleration; $S \cdot l_k \cdot H_c \cdot \frac{dB}{dt}$ – energy dissipated as heat during magnetization reversal; $\frac{dP}{dt}$ - change in magnetic potential energy.

$$\frac{dP}{dt} = S \cdot l_k \cdot (H - H_c) \cdot \frac{dB}{dt} \qquad (4)$$

The magnetomotive force of a magnetic loop is proportional to the current flowing through the coil:

$$I_m \cdot \omega = H \cdot l_k + \frac{2 \cdot \Delta l}{\mu_0} \cdot B \qquad (5)$$

where: $I_m \cdot \omega = I \cdot \omega - I_{ind}$ – magnetization current.

Eddy currents and the current generated by the winding are taken into consideration to determine the magnetization current. According to Faraday-Maxwell's law of electromagnetic induction [16], changes in eddy currents in an electromagnet [3] are described with the following equation:

$$I_{ind} = \frac{S}{R_f} \cdot \frac{dB}{dt} \qquad (6)$$

Equations (1) and (2) can be applied to determine the amount of voltage induced depending on the rate of change in the magnetic field flux:

$$S \cdot \omega \cdot \frac{dB}{dt} = U - R \cdot I \qquad (7)$$

The change in the winding current of a bypass capacitor in the control system can be calculated with the use of the following equation:

$$C_{con} \frac{dU}{dt} = -I. \qquad (8)$$

The above formulas are transformed to produce a system of differential equations:

$$\begin{cases} [T_f + T_{ind}] \cdot \dfrac{dI_m}{dt} = \dfrac{U}{R} - I_m - [T_f + T_{ind}] \cdot \dfrac{2 \cdot B}{\mu_0 \cdot \omega} v_z \\ T_{con} \cdot \dfrac{d(U/R)}{dt} = -I \end{cases} \quad (9)$$

with the following expressions:

$$T_{ind} = \frac{\mu_0 \cdot S \cdot k\mu'}{R_f},$$

$$T_f = \frac{\omega^2 \cdot R_\phi}{R} \cdot T_{ind},$$

$$H_c \cdot l_k + 2 \cdot \Delta l \cdot \frac{B}{\mu_0} = I_m \cdot \omega,$$

$$I = I_m + T_{ind} \cdot \frac{dI_m}{dt} + T_{ind} \cdot \frac{2 \cdot B}{\mu_0 \cdot \omega} \cdot v_{arh},$$

where: S - magnetic pole area: t – time; U – voltage; R – circuit resistance; I – applied current; H_c – magnetic coercivity; l_k – length of magnetic circuit; R_f - winding resistance to ring current; v_{arh} – armature speed; T_f, T_{con}, T_{ind} – time constants for an electromagnet, capacitor, and eddy current, respectively: C_{con} – capacitance (Fig. 2); Δl – air gap.

$$k\mu' = \frac{dB}{dH} \quad (10)$$

The following equation was applied to describe hysteresis in the mathematical model [7, 9, 37]:

$$B = B\left[\frac{H \pm H_c}{kH_c}\right]_{max} \quad (11)$$

where the value of kH_c is determined by the shape of the magnetization curve of a ferromagnetic material.

Changes in magnetization during fuel metering, including the pilot injection, are presented in Figure 11.
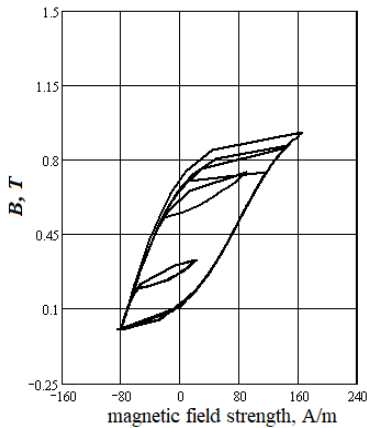

Figure 11. Hysteresis loops for the magnetization and demagnetization of a magnetodielectric material.

The modeled behavior of a solenoid valve was compared with the empirical data (Fig. 12). The presented data were obtained in a magnetic core made of Armco iron. In the empirical study, winding speed was measured with the developed sensor in two different scenarios. In Figure 12a, the modeled results were compared with the performance of the solenoid valve in the absence of hydraulic factors (dry run). In Figure 12b, the modeled results were compared with the real-world performance of the solenoid valve. These comparisons clearly indicate that hydraulic factors determine winding vibrations at the minimal distance from the magnetic circuit. The results of the calculations were compared with the experimental results.
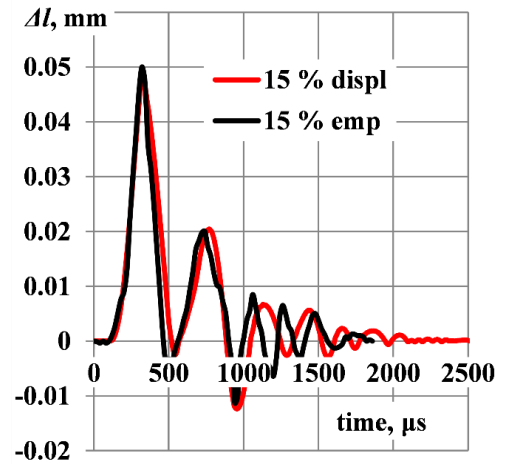
a)
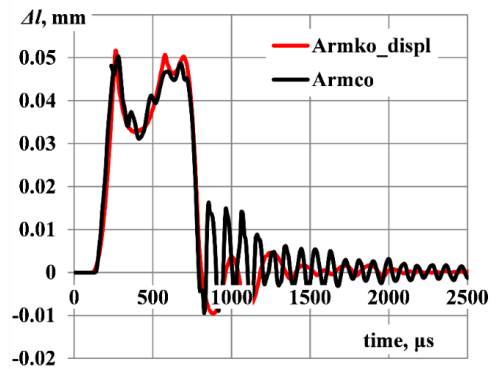
b)

Figure 12. Real-world (emp) and modeled (displ) displacement of the solenoid armature: a) in the test stand (Fig. 7); b) in the injector [32].

The experimental results and the modeled results depict the relationship between winding speed and magnetic field strength (Fig. 13) because these parameters should be analyzed to obtain the required solenoid speed. The relationships between winding speed and magnetic field strength in a two-stage injector (Fig.

13) indicate that a magnetic circuit made of a soft magnetic material (Armco curve) does not generate $C_{arh} > 0.2$ m/s at 50 N. The above threshold should be met to initiate the injection process and inject at least 2 mm^3 of fuel per cycle into the cylinder at a rotational speed of up to 4500 min^{-1}. A hard magnetic material can be incorporated into a soft magnetic core to achieve $C_{arh} > 0.2$ m/s.
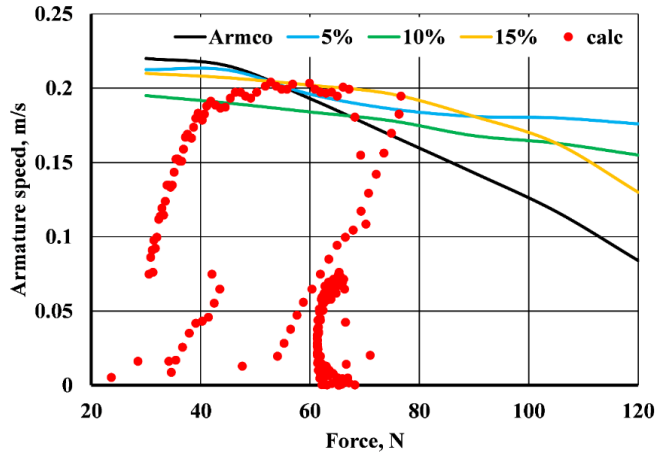

Figure 13. Armature speed in a solenoid valve as a function of magnetic field strength.

4. Conclusions

The results of this study indicate that the magnetic properties of a magnetic core significantly influence valve response times and, consequently, improve fuel injection control. As a result, the fuel can be adequately metered (split into several doses) to improve the parameters of engine performance and decrease greenhouse gas emissions.

The performance of modified magnetic cores was modeled with the use of an equation for determining equilibrium points in a magnet's electric circuit, as well as the time constants of the electromagnet, capacitor, and eddy currents. The results generated by the model were validated in an experiment analyzing the real-world displacement of solenoid armature. These findings can be used to analyze the relationship between armature displacement and initial spring strain. The above

parameters significantly affect the performance of solenoid valve.

The proposed technology for manufacturing magnetic cores with the use of soft magnetic materials, hard magnetic materials, and diamagnetic materials has considerable practical value. The recommended proportions of magnetic materials improve solenoid parameters and reduce eddy currents, which contributes to reliable and precise control of fuel injection.

Further research on increasing the precision of fuel injection in Diesel engines should focus on precise control of the electronic fuel injection system with the use of algorithms for optimizing the control and design of mechatronic systems. The technology for manufacturing magnetic circuits should be also further developed by analyzing materials with different magnetic properties.

Nomenclature

t	Time	s
x	Unit of length	m
I	Applied current	A
S	Magnetic pole area	m^2
U	Voltage	V
R	Circuit resistance	Ω
R_f	Winding resistance	Ω
B	Magnetic flux density	T
H	Magnetic field strength	A/m
H_c	Magnetic coercivity	A/m
ω	Number of coil turns	
σ	Heat transfer coefficient	
μ_0	Vacuum magnetic permeability	N/A^2
μ	Magnetic permeability	N/A^2
C_{con}	Capacitance	F
v	Current velocity	m/s
Δl	Air gap length	m
l_k	Coil length	m
P	Power	W
T	Time constant	s
I_m	Magnetization current	A
Φ	Magnetic flux	Wb
Φ_{arm}	Armature flux	Wb
G	Total magnetic permeability	H/m
g	Magnetic permeability of the air gap	H/m

References

1. Ando R, Koizumi M, Ishikawa T. Development of a simulation method for dynamic characteristics of fuel injector. IEEE Transactions on Magnetics 2001; 37(5): 3715-3718. https://doi.org/10.1109/20.952697.

2. Anfilatov A A, Chuvashev A N. Power and fuel efficiency of a diesel engine with separate feed. Journal of Physics: Conference Series 2020; 1515: 042048. https://doi.org/10.1088/1742-6596/1515/4/042048.

3. Bi X, Wang L, Marignetti F, Zhou M. Research on electromagnetic field, eddy current loss and heat transfer in the end region of

synchronous condenser with different end structures and material properties. Energies 2021; 14: 4636. https://doi.org/10.3390/en14154636.

4. Bor M, Borowczyk T, Karpiuk W, Smolec R. Determination of the response time of new generation electromagnetic injectors as a function of fuel pressure using the internal photoelectric effect. 2018 International Interdisciplinary PhD Workshop 2018: 17859890. https://doi.org/10.1109/IIPHDW.2018.8388385.

5. Borucka A, Kozłowski E, Oleszczuk P, Świderski A. Predictive analysis of the impact of the time of day on road accidents in Poland. Open Engineering 2021; 11(1): 142-150. https://doi.org/10.1515/eng-2021-0017.

6. Borucka A. Method of testing the readiness of means of transport with the use of semi-Markov processes. Transport 2021; 36(1): 75-83. https://doi.org/10.3846/transport.2021.14370.

7. Chan J H, Vladimirescu A, Gao X C, Liebmann P, Valainis J. Nonlinear transformer model for circuit simulation. IEEE Transactions on Computer-Aided Design of Integrated Circuits and Systems 1991; 10(4): 476–482. https://doi.org/10.1109/43.75630.

8. Coppo M, Dongiovanni C, Negri C. Numerical analysis and experimental investigation of a Common Rail-type diesel injector. Transactions of the ASME 2004; 126: 874-885. https://doi.org/10.1115/1.1787502.

9. Detka K, Górecki K. Analiza przydatności metody histerezowej do wyznaczania strat mocy w rdzeniu ferromagnetycznym. Przegląd Elektrotechniczny 2022; 98(9): 139-142. https://doi.org/10.15199/48.2022.09.30.

10. Dimitriadis A, Seljak T, Vihar R, Baškovič U Ž et al. Improving PM-NOx trade-off with paraffinic fuels: A study towards diesel engine optimization with HVO. Fuel 2020; 265: 116921. https://doi.org/10.1016/j.fuel.2019.116921.

11. Dong Q, Yang X, Ni H et al. An on-line measurement method of injection rate of high pressure common rail system. Measurement 2021; 170: 108716. https://doi.org/10.1016/j.measurement.2020.108716.

12. Duda K, Wierzbicki S, Mikulski M et al. Emissions from a medium-duty CRDI engine fueled with diesel-biodiesel blends. Transport Problems 2021; 16(1): 39-49. https://doi.org/10.21307/tp-2021-004.

13. Hu N, Yang J, Zhou P. Sensitivity analysis of the dynamic response of an electronic fuel injector regarding fuel properties and operating conditions. Applied Thermal Engineering 2018; 129: 709-724. https://doi.org/10.1016/j.applthermaleng.2017.10.071.

14. Huber B, Ulbrich H. Modeling and experimental validation of the solenoid valve of a common rail diesel injector. SAE Technical Paper 2014-01-0195. 2014. https://doi.org/10.4271/2014-01-0195.

15. Jaliliantabar F, Ghobadian B, Carlucci A P et al. A comprehensive study on the effect of pilot injection, EGR rate, IMEP and biodiesel characteristics on a CRDI diesel engine. Energy 2020; 194: 116860. https://doi.org/10.1016/j.energy.2019.116860.

16. Kinsler, P. Faraday's law and magnetic induction: cause and effect, experiment and theory. Physics 2020; 2(2): 148–161. https://doi.org/10.3390/physics2020009.

17. Koch R C, Lynch A F, Chladny R R. Modeling and control of solenoid valves for internal combustion engines. IFAC Proceedings Volumes 2002; 35(2): 197–202. https://doi.org/10.1016/s1474-6670(17)33941-1.

18. Martínez-Martínez S, de la Garza OA, García-Yera M, et al. Hydraulic interactions between injection events using multiple injection strategies and a solenoid diesel injector. Energies 2021; 14: 3087. https://doi.org/10.3390/en14113087.

19. Mikulski M, Ambrosewicz-Walacik M, Duda K, Hunicz J. Performance and emission characterization of a common-rail compression-ignition engine fuelled with ternary mixtures of rapeseed oil, pyrolytic oil and diesel. Renew Energy 2020; 148: 739–755. https://doi.org/10.1016/j.renene.2019.10.161.

20. Ovaere M, Proost S. Cost-effective reduction of fossil energy use in the European transport sector: An assessment of the Fit for 55 Package. Energy Policy 2022; 168: 113085. https://doi.org/10.1016/j.enpol.2022.113085.

21. Passarini LC, Pinotti M. A new model for Fast-acting electromagnetic fuel injector analysis and design. J. Braz. Soc. Mech. Sci. & Eng. 2003; 25(1). https://doi.org/10.1590/S1678-58782003000100014.

22. Piron M, Sangha P, Reid G et al. Rapid computer-aided design method for fast-acting solenoid actuators. IEEE Transactions on Industry Applications 1999; 35(5): 991-999. https://doi.org/10.1109/28.793358

23. Pratama R H, Huang W, Moon S. Unveiling needle lift dependence on near-nozzle spray dynamics of diesel injector. Fuel 2021; 285: 119088. https://doi.org/10.1016/j.fuel.2020.119088.

24. Santhosh K, Radheshyam G N K, Sanjay P V. Experimental analysis of performance and emission characteristics of CRDI diesel engine fueled with 1-pentanol/diesel blends with EGR technique. Fuel 2020; 267: 117187. https://doi.org/10.1016/j.fuel.2020.117187.

25. Stelmasiak Z, Larisch J, Pielecha J, Pietras D. Particulate matter emission from dual fuel diesel engine fuelled with natural gas. Polish Maritime Research 2017; 24: 96–104. https://doi.org/10.1515/pomr-2017-0055.

26. Stoeck T. Analytical methodology for testing Common Rail fuel injectors in problematic cases. Diagnostyka 2021; 22(2): 47-52. https://doi.org/10.29354/diag/135999.

27. Stoeck T. Methodology for Common Rail fuel injectors testing in case of non-typical faults. Diagnostyka 2020; 21(2): 25-30. https://doi.org/10.29354/diag/122034.

28. Sun Z Y, Li G X, Wang L et al. Effects of structure parameters on the static electromagnetic characteristics of solenoid valve for an electronic unit pump. Energy Conversion and Management 2016; 113: 119–130. https://doi.org/10.1016/j.enconman.2016.01.031.

29. Szpica D. Validation of indirect methods used in the operational assessment of LPG vapor phase pulse injectors. Measurement 2018; 118: 253-261. https://doi.org/10.1016/j.measurement.2018.01.045.

30. Terzis A, Kirsch M, Vaikuntanathan V, Geppert A, Lamanna G, Weigand B. Splashing characteristics of diesel exhaust fluid (AdBlue) droplets impacting on urea-water solution films. Experimental Thermal and Fluid Science 2019; 102: 152-162. https://doi.org/10.1016/j.expthermflusci.2018.11.002.

31. Tola O J, Obe E S, Obe C T, Anih L U. Finite element analysis of dual stator winding line start permanent magnet synchronous motor. Przegląd Elektrotechniczny 2022; 98(4): 47-52. https://doi.org/10.15199/48.2022.04.11.

32. Vrublevskyi O, Wierzbicki S. Measurement and theoretical analysis of the displacement characteristics of moving components in a solenoid injector in view of wave phenomena. Measurement 2022; 187: 110323. https://doi.org/10.1016/j.measurement.2021.110323.

33. Vrublevskyi O. Modelling of processes in electro-hydraulic valves of an engine' fuel system. Mechanika 2019; 25(2): 141-148. https://doi.org/10.5755/j01.mech.25.2.22015.

34. Więcławski K, Figlus T, Mączak J, Szczurowski K. Method of fuel injector diagnosis based on analysis of current quantities. Sensors 2022; 22: 6735. https://doi.org/10.3390/s22186735.

35. Wierzbicki S, Śmieja M. Visualization of the parameters and changes of signals controlling the operation of Common Rail injectors. Solid State Phenomena 2014; 210: 136-141. https://doi.org/10.4028/www.scientific.net/SSP.210.136.

36. Zhang H, He J, Li S et al. Effect of biodiesel impurities (K, Na, P) on non-catalytic and catalytic activities of Diesel soot in model DPF regeneration conditions. Fuel Processing Technology 2020; 199: 106293. https://doi.org/10.1016/j.fuproc.2019.106293.

37. Zhao J, Fan L, Liu P et al. Investigation on electromagnetic models of high-speed solenoid valve for common rail injector. Mathematical Problems in Engineering 2017: 9078598. https://doi.org/10.1155/2017/9078598.

38. Zhao J, Yue P, Grekhov L, Ma X. Hold current effects on the power losses of high-speed solenoid valve for common-rail injector. Applied Thermal Engineering 2018; 128: 1579–1587. https://doi.org/10.1016/j.applthermaleng.2017.09.123.

39. Zhao J, Yue P, Grekhov L, Wei K, Ma X. Temperature and frequency dependence of electrical iron effects on electromagnetic characteristics of high-speed solenoid valve for common rail injector. International Journal of Applied Electromagnetics and Mechanics 2019; 60(2): 173–185. https://doi.org/10.3233/jae-180022.

40. Zhao J, Yue P, Wei K. Eddy current effects on the dynamic response of high-speed solenoid valve for common rail injector. International Journal of Applied Electromagnetics and Mechanics 2020; 62(3): 607-618. https://doi.org/10.3233/jae-190047.